参加動機と満足度に関する調査結果を，表6に示す．9割近くの受講者が，「現在の仕事・学業に活かすため」と答えているように，明確な動機をもって参加し，高い満足度が得られていることが示された．また，受講者からは，表7に示すコメントが得られている．

② 学習到達度

講義・実習における理解度自己評価の測定結果を，図3，図4にそれぞれ示す．これは，科目ごとに受講前後の理解度回答の平均値を算出したものである．講義・実習ともに，受講者自身の認識において理解度が向上しているように，心理的な抵抗感の払拭につながっている．ここで，変化率は，「変化率＝変化幅／受講前理解度」として算出している．変化率をみると，取り分け，実習による心理的な教育効果が大きい．

講義における知識調査の結果を，図5に示す．これは，科目ごとに回答者全員の平均点（100点満点）を示したものである．全科目において正解率の向上が示された．

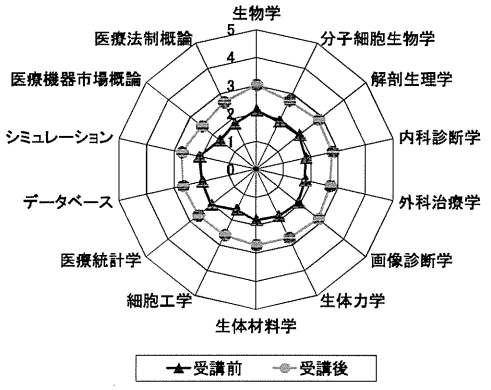

科目	理解度		変化幅	変化率
	受講前	受講後		
生物学	2.11	3.02	0.90	+43%
分子細胞生物学	1.90	2.72	0.83	+44%
解剖生理学	1.96	2.84	0.87	+44%
内科診断学	1.82	2.79	0.97	+53%
外科治療学	1.78	2.70	0.92	+52%
画像診断学	1.93	2.84	0.91	+47%
生体力学	1.85	2.72	0.87	+47%
生体材料学	1.82	2.71	0.88	+49%
細胞工学	1.60	2.61	1.00	+63%
医療統計学	2.04	2.63	0.59	+29%
データベース	1.97	2.68	0.70	+36%
シミュレーション	2.08	2.72	0.64	+30%
医療機器市場概論	1.66	2.47	0.81	+49%
医療法制概論	1.80	2.66	0.86	+48%
講義全体平均	1.88	2.72	0.84	+45%

図 3　理解度自己評価の調査結果（講義）

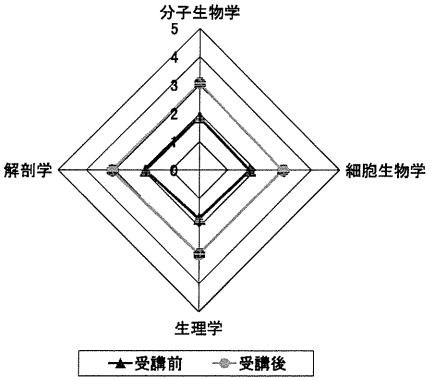

科目	理解度		変化幅	変化率
	受講前	受講後		
分子生物学	1.86	3.07	1.20	+65%
細胞生物学	1.80	2.98	1.18	+65%
生理学	1.71	2.95	1.25	+73%
解剖学	1.91	3.09	1.18	+62%
実習全体平均	1.82	3.02	1.20	+66%

図 4　理解度自己評価の調査結果（実習）

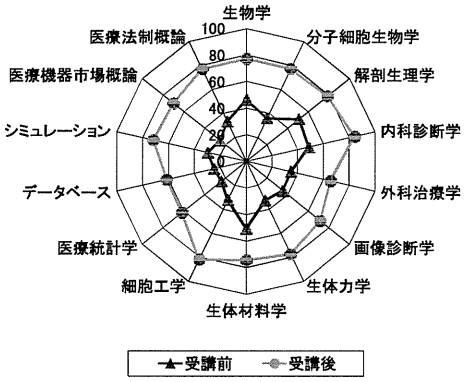

科目	平均点		変化幅	変化率
	受講前	受講後		
生物学	46.4	77.1	30.8	+66%
分子細胞生物学	36.0	77.3	41.2	+114%
解剖生理学	51.1	78.6	27.6	+54%
内科診断学	48.6	84.1	35.6	+73%
外科治療学	34.7	65.6	30.9	+89%
画像診断学	35.3	71.6	36.3	+103%
生体力学	32.7	77.3	44.7	+137%
生体材料学	50.6	74.2	23.6	+47%
細胞工学	32.0	81.7	49.7	+155%
医療統計学	24.0	61.8	37.8	+157%
データベース	25.0	61.4	36.4	+146%
シミュレーション	29.8	71.8	42.0	+141%
医療機器市場概論	25.4	70.1	44.7	+176%
医療法制概論	33.2	77.0	43.8	+132%
講義全体	36.1	73.5	37.5	+104%

図 5　知識調査結果

③ 行動変容度

科目別の活用状況に関する調査結果を，図6に示す．所属企業に戻った後，特に業務に役立った科目として，解剖と実習を挙げる声が大きい．また，具体的な業務活用事例として，表8に示す受講者のコメントが得られている．この調査によって，カリキュラムの受講を通じた一

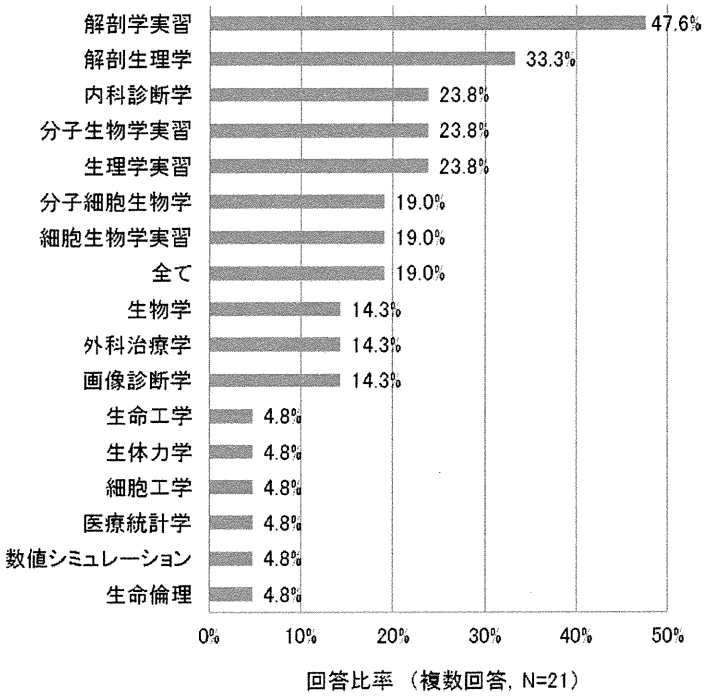

図 6　科目活用状況に関する調査結果

表 8　業務活用状況に関する受講者のコメント

(役に立った事例)
・ 医師との専門用語を交えた会話の理解にも役立った.
・ 営業部門や医師の要求仕様を設計開発に反映させる際に必要となる専門用語, 特に臨床に関する知識が理解できた.
・ エコー診断設備開発, CT スキャンや MRI の開発仕様を作成する上で役立った. 特に, 競合する他社製品に対する機能の優位性を評価する見方や知識を得た.
・ 超音波診断の解析チームに所属しているが, 臓器の部位, 生体の構造を理解する上で, ターゲット臓器の構造, 腹腔内の空気や骨格を事前に把握することが可能になった.
・ 工学偏重の考え方から脱却して, 医学分野への視野も拡大した.
・ 知識を習得する為の手法や手掛かりを得た. 特に大学教授陣による研究事例の紹介では, 医療機器の開発や研究に関する視野の拡がりを感じた.
・ 社内でのバイオテクノロジーに関するワーキンググループで議論に供しうる知識を得た.
・ 医療系情報システムの開発, 構築に従事しており, ユーザーの専門用語を理解する手助けとなった.
(その他の意見)
・ 当社は, 医学の基礎知識取得を目的として参加したので, 直接的に業務の役に立ったことはない.
・ 具体例としては, 特にない. 「広く, 浅く」という, 本再教育プログラムの性格から即効性を期待していない.

定の行動変化が確認され，行動面につながる教育効果が明らかになった．

④ 評価のまとめ

以上の調査によって，心理的側面・知識的側面における学習効果，および，受講満足度の高さが明らかになった．また，カリキュラムの受講を経て，一定の行動変容にもつながっていることが明らかになった．今後の継続的な開催や，さらなる拡充を望む声が大きいことからも，社会人のための再教育システムへの需要や期待が伺えた．取りわけ，REDEEMにおいては，解剖学をはじめとした実習による体験的

学習の機会が，カリキュラムを特長付ける内容として認識された．

2）カリキュラムの再開発の結果

① 実証研究結果のフィードバック

以上の実証研究で得られた知見をフィードバックして，第2期REDEEMの再開発をおこなった．全体構成ついては，第1期の方針を継続し，第2期においても，実験・実習を中核としてその前提となる生物学や基礎医学の講義を重点的におこなう．講義科目については，要望を踏まえて，基礎医学や臨床医学の内容を充実させる．また，ESTEEMの実証研究[10]よって産業界の要望が明らかになった，医療法制・医療機器市場に関する講義を追加する．開催方法については，大半の受講者が希望する集中プログラムの形態[15]を継続する．また，関東からの参加者が多数を占める傾向にあることから，出張講義も継続する．

② 教 育 目 標

教育目標は，次のとおり設定した．

・産業社会の第一線において，研究・開発にあたっている社会人技術者に対して，生物学・医学・医工学の基礎教育をおこない，医療工学産業を創成できる人材を創り出す．
・創成される人材は，医療の実践現場において，医師・医療従事者と対等なパートナーとして医療工学の技術開発・研究にあたる．
・網羅的な知識ではなく，生物学・医学・医工学の考え方のエッセンスを，工学技術の言葉・体系で伝え，研究・開発の自律的発展の基礎とする．
・空理・空論を排し，実験・実習を通じ，経験に裏付けられた知識と技術の獲得を目指す．

③ 開 催 方 法

開催方法は，次の構成を基本とすることとした．

・集中講義
　日程：年2回，各回1週（5日）開催
　会場：東北大学工学部内（仙台市）
　定員：各回50名程度
・出張講義
　日程：年10回，月1日開催（シンポジウム開催月を除く毎月）
　会場：学術総合センター（東京都）

表9 第2期 REDEEM の科目構成

区分		科目名	コマ数	
			必修	選択
1. 講義	基礎生物学	生物学	2	
		分子細胞生物学	4	
	基礎医学	人体解剖生理学	14	
	臨床医学	内科学		4
		外科学		4
		画像診断学		3
	医工学	医工学の基礎		2
		生体工学		2
		シミュレーション医工学		1
		生体材料学		1
	医療法制・医療機器市場	医療法制・薬事法		2
		医療機器市場概論		1
		実験・実習ガイダンス	1	
2. 実習		分子生物学実験	6	
		細胞生物学実験	6	
		生理学実験	2	
		解剖学実習	6	
3. シンポジウム		(最先端の医工学テーマ)		3
計			41	20

定員：各回50名程度

・実　　習

日程：年2回，各回1週（5日）開催

会場：東北大学医学部内（仙台市）

定員：各回18名

④科目構成

年度あたりの科目構成を，表9に示す．カリキュラムは，講義合計41コマ，実習合計20コマにより構成し，年1回のシンポジウムは，講義3コマ分と見なすこととした．講義は，修了認定のために必要となる必修科目，および，希望に応じて受講できる選択科目で構成する．

4．考　　察

この社会人再教育のためのカリキュラムは，学位取得を目指す大学院教育とは異なり，実務家のための専門コースと位置付けている．産業界などから参加した受講者の声を反映した集中的プログラムによる構成は，本カリキュラムの特徴の1つである．研究・開発などの場面で専門性を広げる必要性に迫られた人材が，実務から長期間離れることなく，効果的に新たな技術や知識を獲得するための入り口になるものと考えられる．このような社会へ開かれた再教育システムへの需要，取りわけ，医工連携分野に関しては，産業界では得がたい生物学や医学系科目の学習機会が求められている．

本研究で示されたように，REDEEMの受講者の満足度は非常に高い．また，ESTEEMにおいても同様の実証研究結果が得られている[10]．毎年受講者を派遣している企業もあるように，今後の継続実施が望まれるところである．また，定員を超える受講状況からも，需要の大きさを示すところとなった．これらの結果を総合すると，医工学の再教育カリキュラムの需要は大きく，産業界の声を反映したカリキュラム開発および学習機会の提供は，今後益々，重要となってくるものと考えられる．

今後，これらの実証研究を通じて開発してきた，基礎カリキュラムREDEEMと上位カリキュラムESTEEMを，体系付けて連携させた社会人再教育コースとして整備することが，次のステップとして期待される．また，以上に述べてきた「社会人を対象とした医工学の人材育成拠点」という主たる目的に加えて，「医工学の産学人材交流拠点」へ発展する可能性を有する．人材育成の仕組みを中核に，医工学に関する産学人材交流拠点として，産学連携の研究・事業協力，大学を通じた企業間連携，先端的取り組みの啓蒙活動など，医工学人材ネットワークを構築するハブ（HUB）としての機能が構想される．これまでの取り組みにおいて，REDEEM受講者を中心とした，「REDEEM協議会」という会員組織が設置されている．これまでは，シンポジウムの開催に準じた活動に限定されているが，今後の機能拡張が足掛かりとなるように考えられる．

以上のように，特色あるカリキュラムを中心として，人が集まり交流する仕組み，また，産業界と大学が相互に学ぶ産学連携の仕組みを整えていくことが，再教育システムの付加価値となり，今後の発展の方向性となるのではないかと考えられる．

5．結　　論

本論文では，わが国の医療機器産業を担う社会人技術者を主要対象とした，医工学カリキュラムREDEEMの開発・実施・評価を通じて，その需要と効果について示した．そして，研究結果をフィードバックして再開発した第2期REDEEMと，再教育システムの将来展望について述べた．

この実証研究において明らかになったのは，実践的・体験的な学習機会への需要の高さである．取りわけ，本カリキュラムで主要対象とした，医療機器産業の社会人技術者の再教育に関しては，産業界では得がたい生体・医学系の体験学習機会に対する期待が非常に大きい．実際に手を動かす実践的・体験的学習は，プログラムを特色付ける主要な要因となり，今後，さまざまな医工学分野へのニーズが広がるのではないかと考えられる．

ひいては，このような人材育成プログラムから輩出された技術者・研究者によって，わが国の医療機器産業の発展が先導されていくものと期待される．結論として，医療機器産業を担う

社会人技術者を主要対象とした医工学における再教育システムは，今後の医療機器産業や医工学の発展にとって非常に価値のある仕組みであると考えられる．

なお，平成22年度現在，本稿で紹介した第2期REDEEMでは，随時，受講者の受け入れがおこなわれている．関心をお持ちの方は，ウェブサイト（http://www.redeem.jp/）までアクセスされたい．

謝　辞

実証研究の推進にあたり，産学より参画頂いた運営委員および講師の先生方，また，受講者として貴重なご意見を頂いた皆様方に，心より感謝の意を表します．また，本研究の遂行にあたり，文部科学省の支援を頂きました．ここに厚く御礼申し上げます．

文　献

1）総合科学技術会議. http://www8.cao.go.jp/cstp/index.html (参照 2010).
2）文部科学省グローバルCOEプログラム. “新世紀世界の成長焦点に築くナノ医工学拠点”. http://www.nanobme.org/ (参照 2007).
3）東北大学大学院医工学研究科. http://www.bme.tohoku.ac.jp/ (参照 2008).
4）山口隆美. 医療工学－工学による医療の再編－小特集号発刊に際して. 日本機械学会誌. 2006, Vol. 109, No. 1,047, p. 85.
5）山口隆美, 山野真裕. バイオエンジニリング教育. 機械の研究 (養賢堂). 2010, Vol. 62, No. 1 , p. 169-174.
6）経済産業省バイオ人材育成システム開発事業. “医療工学の指導的人材の育成”. http://www.redeem.jp/h14bio/ (参照 2003).
7）文部科学省科学技術振興調整費 ・ 新興分野人材養成 “医療工学技術者創成のための再教育システム”. http://www.redeem.jp/ (参照 2004).
8）経済産業省産学連携製造中核人材育成事業. “次世代医療関連産業中核人材育成のための実践的教育システム”. http://www.redeem-esteem.jp/ (参照 2006).
9）山野真裕, 松木範明, 沼山恵子ほか. 東北大学における「医療工学技術者創成のための再教育システム」の実践. 工学教育. 2008, Vol. 56, No. 6 , p. 125-132.
10）山野真裕, 松木範明, 沼山恵子ほか.「次世代医療関連産業中核人材育成のための実践的教育システム」の開発と実証研究. 工学教育. 2009, Vol. 57, No. 2 , p. 13-21.
11）Noriaki Matsuki.; Motohiro Takeda.; Masahiro Yamano. et al. Effects of unique biomedical education programs for engineers. REDEEM and ESTEEM projects. Advan Physiol Educ. 2009, 33, p. 91-97.
12）Noriaki Matsuki.; Motohiro Takeda.; Masahiro Yamano. et al. Designing a clinical education program for engineers. The ESTEEM Project. Journal of Interprofessional Care. 2010, Vol. 24, No. 6 , p. 738-741.
13）Kirkpatrick,D.L. “Techniques for Evaluating Training Programs” in Evaluating Training Programs. Alexandria. VA. American Society for Training and Development. 1975, p. 1 -17.
14）(独)雇用・能力開発機構 職業能力開発総合大学校能力開発研究センター：公共能力開発施設の行う訓練効果測定－訓練効果測定に関する調査・研究－. 2005.
15）東北大学, アドバンスソフト株式会社. 平成14年度補正事業経済産業省バイオ人材育成システム開発事業「医療工学の指導的人材の育成」報告書. 2004.

J Mol Model (2011) 17:2773–2780
DOI 10.1007/s00894-010-0946-7

ORIGINAL PAPER

Adsorption mechanism of single guanine and thymine on single-walled carbon nanotubes

Muthusivarajan Rajarajeswari · Kombiah Iyakutti · Yoshiyuki Kawazoe

Received: 2 November 2010 / Accepted: 27 December 2010 / Published online: 29 January 2011

Abstract Bio-nano hybrids introduce magnificent applications of nanomaterials to various fields. The choice of carbon nanotube as well as sequence selection of the nucleic acid bases play a crucial role in shaping DNA–carbon nanotube hybrids. To come up with a clear vision for the choice of carbon nanotube and nucleic acid bases to create bio-nano hybrids, we studied the adsorption mechanism of the nucleic acid bases guanine and thymine on four different types of nanotubes based on density functional theory. Nucleic acid bases exhibit differential binding strengths according to their structural geometry, inter-molecular distances, the carbon nanotube diameter, and charge transfer. The π–π interaction mechanism between the adsorbent and adsorbate is discussed in terms of charge density profile and electronic band structure analysis.

Keywords Carbon nanotube · Nucleic acid base · π–π stacking interaction · Density functional theory

Introduction

The study of the noncovalent interactions of biological molecules with single-walled carbon nanotubes (SWCNT) has emerged as a separate field in nanotechnology. Functionalization of CNT with biomolecules leads to many potential applications in medicinal biology as well as in solid state nano electronics. Carbon nanotubes are being explored as one of the most promising transfection vectors for drug and gene delivery, due to their large surface area, stability, flexibility and biocompatibility. Hybrids of SWCNT-ribonucleic acid (RNA) polymer formed through nonspecific binding are translocated into MCF7 breast cancer cells with radioscope labeling [1]. SWNTs have the ability to penetrate mammalian cells as intracellular protein transporters with noncovalently bound protein cargo [2]. An electronic biosensor for detecting antibodies associated with human autoimmune diseases has been developed through the nonspecific binding of proteins on carbon nanotubes [3]. Carbon nanotubes decorated with peptide is used in a field effect transistor (FET)-based chemical sensor to detect specific targets using peptide recognition elements [4].

Deoxyribonucleic acid (DNA) overstated its role not only in biology, but also in nanotechnology. Integration of carbon nanotubes with the genetic material DNA opens up several possible applications of CNT in the field of bio-nanotechnology. Over a decade of research has now contributed to our understanding of the interactions in DNA–CNT hybrids. Nonspecific interaction of CNTs with DNA helps the dispersion and separation of CNTs in aqueous and non-aqueous solution, while leaving the unique physical and electronic properties of CNTs unchanged. The helical wrapping of poly(T) on a carbon nanotube (10, 0) converts CNT into a water soluble object and helps to sort the carbon nanotubes with respect to their electronic properties [5]. Self-assembly of the sequence $d(GT)_n$ around individual nanotubes enables nanotube separation using ion exchange liquid chromatography [6, 7]. In the study of a

M. Rajarajeswari · K. Iyakutti (✉)
School of Physics, Madurai Kamaraj University,
Madurai, Tamil Nadu 625 021, India
e-mail: iyakutti@yahoo.co.in

Y. Kawazoe
Institute for Materials Research, Tohoku University,
Sendai 980-8577, Japan

molecular dynamics simulation of a self-assembly of random sequence ssDNA on CNT, achiral loops and disordered kinked structures are observed due to the flexibility of ssDNA [8]. Also, the helical wrapping of poly (GT) on CNT [6, 7] is claimed to be structurally unstable, and the oligonucleotide does not prefer to be adsorbed onto CNTs as a dimer. "Ultrasoft" DNA sequencing have been performed by detecting the variation in the current through a CNT when different DNA base pairs are in contact with the CNT [9]; the individual nucleosides adsorbed on the CNT are also identified with the applied external gate voltage [10]. These results shows that the adsorption mechanism of nucleic acid bases on CNT varies with respect to each nucleic acid base. Depending on the length and the sequence of nucleic acid bases in the DNA, a large molecular library is available from which to produce a number of DNA–CNT hybrids, leading to a wider range of magnificent applications. In its simplest form, individual nucleic acid bases can interact with CNTs singly or in multiples (poly). Interactions of isolated nucleic acid bases with CNTs have been studied using density functional theory (DFT) with different functionals [11, 12], and with Raman spectroscopic technique [13]. Das et al. [14] investigated the binding of nucleobases with CNT by means of Hartree-Fock (HF) theory and isothermal calorimetry experiments. Atomistic molecular dynamics (MD) simulations were performed to study the binding of nucleotide monophosphates with (6, 0) SWCNTs in aqueous solution [15]. From previous reports, it is clear that generally binding of DNA to CNT depends generally on the nucleotide sequence and the nanotube diameter [16].

In earlier reports, binding energies of all five nucleic acid bases with a carbon nanotube is calculated using different density functional codes [11–17]. Interaction strength varies in the order G>A>T>C>U [11, 13, 14]. Self-stacking interactions of nucleobases compete with the cross-stacking interaction strength of nucleobases with CNT [18]. Thus, the interaction strength of nucleobases with CNT should be able to overcome the self-stacking interactions. Using ion exchange chromatography technique, Zheng et al. [5–7] proved the ability of poly (T) and poly (GT) to disperse CNTs in aqueous solution. Of the four nucleobases, from the relative binding energies of self-stacking nucleobases and cross-stacking on CNT, Wang [18] proved that thymine can disperse CNT in aqueous solution better than adenine and cytosine. Consequently, the nucleic acid bases thymine and guanine have gained importance in the dispersion of CNTs. Like the differential adsorption strength of nucleic acid bases, different chiralities of CNT also play a significant role in the binding strength of CNT–nucleic acid base hybrids. Earlier reports concentrated on finding the variation in binding energies of different nucleic acid bases with a CNT. Some reports presented electronic band structure analysis and iso surface charge density plots [11, 17], and examined the interaction between them. However, we choose to investigate the role of the curvature and chirality of the CNT in the formation of DNA–CNT hybrid. In our study, to expand our knowledge of the interaction between the nucleic acid bases thymine and guanine and CNTs of different chiralities, with the help of standard density functional code, we present the role of geometry, adsorption mechanism, charge transfer, electronic band structure analysis and charge density analysis.

Computational details

Calculations were carried out using DFT with a plane wave basis set as implemented in the Vienna ab-initio simulation package (VASP) [19, 20]. The projected augmented-wave method (PAW) is used to describe the interaction between ions and electrons [21]. The PAW method has two advantages over ultrasoft pseudo potentials (USPP). It provides all-electron wave functions for valence electrons and shows a better convergence behavior than USPP [21]. DFT is used to describe the ground state properties of many-body systems. Exchange correlation energy can be evaluated with the help of local density approximation (LDA) [22] or with generalized gradient approximation (GGA) [23]. Non-covalent interaction between the two systems is the result of van der Waals, hydrogen bonding, ion-pairing, cation–π and π–π interactions. It is well known that neither LDA nor GGA can describe weakly bound systems perfectly. A considerable effect of exchange correlation energy functionals in the binding energy was noted with DFT techniques. Generally, LDA overestimates the interaction energy of weakly bound systems and GGA underestimates it. Here, our aim was to study non-covalent interactions between DNA–CNT hybrids, thus we had to be very precise in choosing an exchange correlation functional with which to determine accurate interaction energies and structural properties. DFT-LDA calculations underestimate dispersion energy at large distances but can reproduce the empirical potential for graphitic structures successfully [24]. Studies on self-stacking of benzene and cross stacking of benzene on graphene sheet within GGA have shown almost no binding energy [25]. However, the interlayer distance for adenine adsorption on graphene sheet reported using the DFT-LDA technique is very close to the experimental result [26]. Most recently, Lim and Park [27] have investigated the noncovalent adsorption of aromatic molecules on CNT with the help of LDA, GGA and hybrid functionals. It was found that DFT-LDA and M06 hybrid functionals produce almost equal binding energy, and that GGA fails to predict the noncovalent interaction. With this

previous literature support, we decided to follow the LDA approach to investigate the exchange correlation energy of our weakly bound systems.

For k-points sampling of the brillouin zone, a 1×1×4 Monkhorst-Pack grid [28] is used with a spacing of 0.025 $Å^{-1}$. For the electronic band structure calculations, 41 irreducible k-points are considered along the *z*-axis direction. Cutoff energy for the plane wave basis set of the valence electron was fixed as 500 eV throughout the calculations. Residual minimization / direct inversion in the iterative subspace method (RMM–DIIS) is used for wave function optimization. Geometry optimization was carried out until the magnitude of the forces acting on all atoms was smaller than 0.0005 eV/Å. The CNTs zigzag (5, 0), (10, 0), armchair (5, 5) and chiral (5, 2) were used in this study. The number of unit cells of CNT is limited by the height of the nucleic acid bases. In all four cases, approximately 20 Å distance is kept between adjacent tubes to avoid interactions between them. Thymine and guanine are nucleic acid bases found in the genetic material DNA. Thymine is a pyrimidine nucleobase, having one hexagon ring with two nitrogen atoms. Guanine is a derivative of purine consisting of a fused pyrimidine-imidazole system with conjugated double bonds. Initially, the hexagon of the nucleic acid base is kept head-to-head with the hexagon of the carbon nanotube. The plane of the nucleic acid base is parallel with the nanotube *z*-axis direction. Atoms are allowed to relax freely in all directions, to determine the possible adsorption positions of nucleic acid bases on the CNT surface.

Results and discussion

Geometry and energetics of adsorption of guanine and thymine on SWCNTs

Prediction of accurate interaction energy of the adsorbate with the adsorbent involves description of intermolecular parameters such as the orientation of the adsorbate, and inter-molecular distances between the adsorbent and adsorbate. These parameters play a significant role, especially in the case of non-covalent interactions. During geometry optimization, the initial orientation of nucleic acid bases on CNTs was altered to attain the minimum energy configuration, but the nucleic acid bases are still parallel to the nanotube surface. The distance between the CNT and each nucleic acid base is measured from the center of the hexagonal ring of the adsorbate to the nanotube surface. Binding energies, equilibrium distances and charge transfer from the nucleic acid bases to the CNT are presented in Table 1. There is no chemical bond formation between the systems and the binding energies confirm that the process is physisorption. The oxygen and nitrogen atoms of nucleic acid bases have lone pairs of electrons and, due to the sp^2 hybridization of carbon atoms in the CNT, each carbon atom possesses one delocalized p electron. These π electrons lead to physisorption of the nucleic acid bases on the CNT.

Intermolecular distances between the CNT and the nucleic acid bases guanine and thymine vary between 2.46 and 3.26 Å. These values are comparable to those reported in previous studies [13, 17]. Among the four nanotubes, thymine is adsorbed close to CNT (10, 0) at a distance of 2.46 Å, which is less than the characteristic π–π stacking distance. Intermolecular separation of adenine on graphite surface is reported as 3.1 Å within LDA, and AFM studies give the same value [26]. As reported by Stepanian et al. [13], the difference between intermolecular distances estimated using second-order Moller-Plesset perturbation theory (MP2) and DFT is about 0.02 Å. Thus, the calculated intermolecular separation of a non-covalently bound system using DFT-LDA is comparable with the results obtained from experiments and MP2 methods. Adsorption of nucleic acid bases on CNT resembles AB stacking between graphene layers. The orientation of nucleic acid bases on the surface of the CNT differs with

Table 1 Binding energies, charge transfer, equilibrium distances for the adsorption of guanine and thymine on carbon nanotubes (CNTs), and diameter of CNTs

System	Binding energy (E_b, eV)	Charge transfer from nucleic acid base (q, e)	Distance (d, Å)	Diameter (d_t, Å)
CNT (5, 0)+Guanine	0.41	0.094	3.07	3.96
CNT (5, 2)+Guanine	0.36	0.009	3.05	4.95
CNT (5, 5)+Guanine	0.38	0.001	2.98	6.87
CNT (10, 0)+Guanine	0.39	0.008	3.06	7.94
CNT (5, 0)+Thymine	0.20	0.026	3.26	3.96
CNT (5, 2)+Thymine	0.26	0.005	2.95	4.95
CNT (5, 5)+Thymine	0.30	0.009	2.97	6.87
CNT (10, 0)+Thymine	0.20	0.014	2.46	7.94

CNT chirality so as to attain the minimal energy configuration.

The binding energy of guanine with a narrow nanotube (5, 0) is 0.41 eV, and the tube becomes compressed in the direction of the adsorbate. The radius of the tube is reduced to 1.87Å in the strained direction (Fig. 1a,e). In studies of interaction between nanotubes and biomolecules, to reduce the computational expense, fragmented CNTs have been used [13, 18]. Fragmenting material such as high-curvature CNT may not give reliable results. Wang [18] examined the adsorption of DNA nucleic acid bases with fragments derived from CNTs (5, 5) and (10, 0). The CNT fragments were frozen with saturated H atoms, thus limiting the interaction of the CNT with the nucleic acid base. This will surely affect the binding energy of the nucleic acid base, whereas we have taken the fully relaxed CNT and allowed all the atoms to move freely in all three directions. Wang [18] reported more than one stable configuration of nucleic acid base on CNT, with a binding energy for guanine varying from 0.32 to 0.44 eV for CNT (5, 5) and from 0.22 to 0.34 eV for CNT (10, 0) without basis set superposition error (BSSE) correction. In another study using MP2 level theory, binding energies of guanine with CNT (5, 5) in the order of 0.36 to 0.88 eV were reported [13]. The curvature-free surface of graphene facilitates the adsorption of planar molecules compared to narrow nanotubes [29]. Except in the case of CNT (5, 0), the binding energy of guanine increases with increasing CNT diameter (Table 1).

Optimized structures of CNT+thymine complexes are presented in Fig. 2. The parallel orientation of thymine helps the interaction between the π orbitals of CNT and thymine. In the adsorption of thymine on CNT (5, 0), the upper half of thymine gets very close to the CNT (Fig. 2e). The lone pair of electrons present in the nitrogen and oxygen atoms caused a tilt in the parallel orientation of thymine on the CNT surface but still the thymine remains planar without pyramidalization. Due to π electron cloud interactions between the CNT and thymine, the CNT becomes distorted in the direction of the adsorbate, like in the CNT (5, 0)+G complex. Here the radius of the (5, 0) tube shrinks to 1.92Å. In the other three cases , the adsorbate does not lead to any change in the CNT structure. Wang [18] analyzed the ability of thymine to disperse SWCNTs by investigating the adsorption of nucleic acid bases on CNT in the gas and aqueous phases. The reported binding energies in the gas phase using MPWBIK functional are in the range of 0.11 to 0.29 eV for the different orientations of thymine on CNT (5, 5), and these values agree well with our results (Table 1).

CNT (10, 0) is a wide tube, with a lesser curvature effect compared to the other nanotubes considered in this study. The binding energy of thymine with CNT (10, 0) is 0.20 eV. In a study of the interaction of thymine/thymine radicals with CNT (10, 0) [17], binding energies in the order of 0.22 to 0.31 eV are reported, which is comparable with our results. However, the binding energy of thymine with CNT (10, 0) is expected to be higher than the other narrow nanotubes. In the optimized structure of CNT (10, 0)+T (Fig. 2d), thymine is positioned at a distance of 2.46Å. This is the shortest intermolecular distance of all the nanotubes tested here. Two CO and NH groups of thymine are tilted towards the CNT. The intermolecular distance between the adsorbent and adsorbate plays a key role in the π-stacking interaction. The π–π repulsive interaction between the adsorbent and adsorbate causes the system to have a certain distance of separation called the characteristic distance of π-stacking, so as to minimize the exchange repulsive interaction between them. Electronegative oxygen and nitrogen atoms present in thymine are thus dragged towards the CNT; this increases the repulsive interaction between the thymine and the CNT and results a considerable reduction in the binding energy.

Generally, π–π interaction energy is the result of electrostatic, induction, charge transfer, dispersion and repulsive energies between the adsorbent and adsorbate [30]. DFT fails to describe the dispersion interaction of

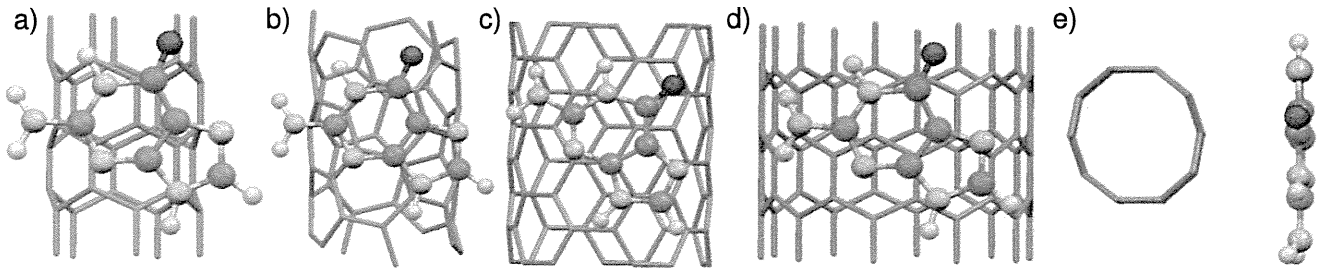

Fig. 1a–e Optimized configurations of guanine adsorbed on carbon nanotubes (CNTs). **a** CNT (5, 0)+G; **b** CNT (5, 2)+G; **c** CNT (5, 5)+G; **d** CNT (10, 0)+G; **e** CNT (5, 0)+G

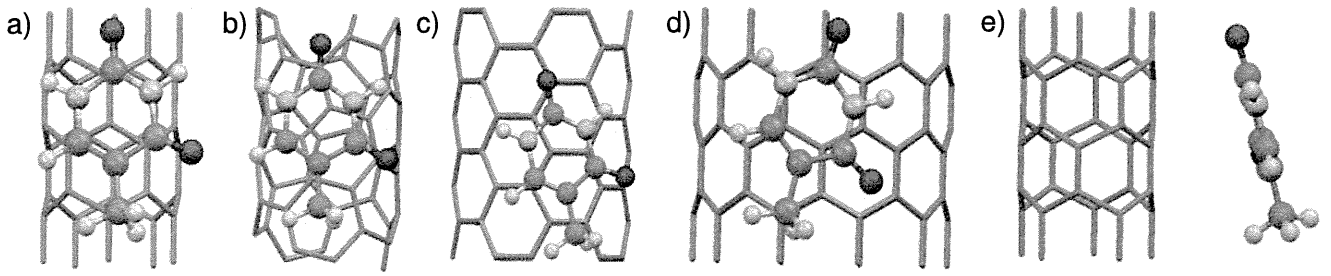

Fig. 2a–e Optimized configurations of thymine adsorbed on CNTs. **a** CNT (5, 0)+T; **b** CNT (5, 2)+T; **c** CNT (5, 5)+T; **d** CNT (10, 0)+T; **e** CNT (5, 0)+T

noncovalent systems at very large distances. Calculating the interaction energy perturbatively using symmetry-adapted perturbation theory (SAPT) [31] can describe such intermolecular interactions, including dispersion energy. SAPT interaction energy is expressed as the sum of electrostatic, exchange, induction, exchange-induction, dispersion and exchange-dispersion components. It is a very successful technique for molecules of ten atoms or fewer but is not suitable for large systems. In our case, the intermolecular separation between CNT and nucleic acid base varies between 2.46 and 3.26 Å. With this intermolecular separation, DFT-LDA can determine the interaction energy of the noncovalent system successfully [24]. Here, the binding energy results from electrostatic, induction, charge transfer and repulsive interactions.

Charge transfer and charge density analysis

Bader charge density analysis [32] was performed to determine the total charge associated with each atom and to investigate possible charge transformation between the two entities. Although there is no direct chemical bonding between the adsorbate and CNT, we can expect a fractional charge transfer between them due to the π electrons and lone pair of electrons. In a similar situation, Stepanian et al. [13] observed a downshift of G-band frequency in the Raman spectra due to partial charge transfer to the nanotube from the nucleic acid base. In our case, a charge of 0.09e is transferred to CNT (5, 0) from guanine (Table 1); this validates the higher binding energy of guanine with the narrow tube rather than the wide tubes. The high curvature surface and the increased electronegativity of CNT (5, 0) drag more electrons towards it [10]. In the other cases, there is no significant charge transfer.

In some earlier works, charge transfer between the CNT and the nucleic acid base was calculated [11, 14, 17, 18] and isosurface plots [11, 17] were examined. Physisorption of nucleic acid bases with CNT occurs due to the interaction between the π electron clouds. Thus, by concentrating on the complete charge density profile of CNT and nucleic acid bases, we will be able to give a better interpretation about the nature of the interaction between them. We analyzed [33] the highest occupied molecular orbital (HOMO) and lowest unoccupied molecular orbital (LUMO) surfaces of CNT and nucleic acid bases. Here, we present the results of two important as well as unique cases: adsorption of guanine on CNT (5, 0) and adsorption of thymine on CNT (10, 0). Figure 3 shows the charge density distribution of the isolated guanine molecule and CNT (5, 0) guanine hybrid.

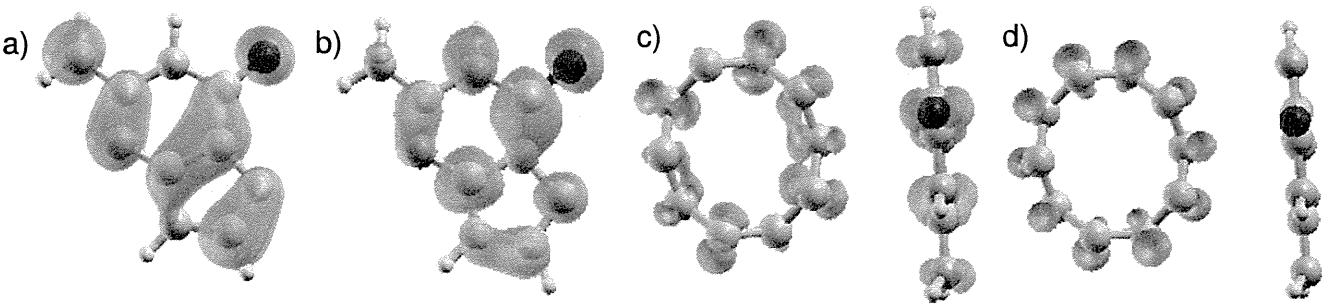

Fig. 3a–d Charge distribution in the CNT (5, 0) guanine hybrid. **a** Highest occupied molecular orbital (HOMO) of isolated guanine. **b** Lowest unoccupied molecular orbital (LUMO) of isolated guanine. **c** HOMO of CNT (5, 0) guanine hybrid. **d** LUMO of CNT (5, 0) guanine hybrid

Charge density is concentrated on the C–C and C–N bonds of the isolated HOMO guanine (Fig. 3a), and in LUMO (Fig. 3b) it spreads over all the atoms. Contribution of the delocalized π electrons of the CNT in the interaction is clearly visible in the bottom panel pictures. Contraction of the CNT diameter near the adsorption field disturbs the π electron distribution over the carbon atoms (Fig. 3c). Thus there is depletion in the charge density of HOMO, whereas in LUMO charge is distributed homogeneously throughout the CNT (Fig. 3d). HOMO charge density concentrated on the guanine triggers physisorption with CNT. Charge accumulated on the oxygen and C–N bonds of guanine induces charge transfer to CNT. HOMO and LUMO of isolated thymine and the CNT (10, 0) thymine hybrid are presented in Fig. 4. In the HOMO of the isolated molecule (Fig. 4a), the charge density is evenly distributed over the carbon, nitrogen and oxygen atoms. Accurate geometry optimization plays a crucial role in the study of non-covalent interactions. During the adsorption of thymine on CNT (10, 0), thymine tilts towards the CNT along the side with two oxygen atoms. In the HOMO (Fig. 4c) of CNT (10, 0)+Thymine, a large collection of π electron density is gathered on the CNT near the thymine. Also, some small amount of charge accumulates on the base. Thus, the interaction between the π electron clouds is repulsive, and reduces the binding strength between the two entities.

Electronic band structure and density of state analysis

Generally, the electronic property of a CNT is not modified by physisorption of the adsorbate [11, 17]. Figure 5 shows the electronic band structure and density of states plots for the CNT (5, 0) and CNT (5, 0) guanine hybrid and CNT (5, 0) thymine hybrid, respectively. Intrinsic CNT exhibits metallic characteristics; the adsorption of neither guanine nor thymine changes the electronic properties of CNT (5, 0). However, the adsorption of the nucleic acid bases introduced additional bands below −0.5 eV in the intrinsic CNT band structure. In the DOS plot, no changes were observed at the Fermi level, confirming that the adsorption of nucleic acid bases on CNT is a simple superposition of individual systems without hybridization of orbitals. This holds true for all the other cases too.

Interaction of guanine thymine pair with CNT (5, 0)

In addition to the study of the adsorption of isolated bases on CNT, adsorption of a single guanine-thymine (GT) wobble base pair on CNT (5, 0) was investigated. A GT wobble base pair is formed with two hydrogen bonds between the O–H–N atoms of the bases [8]. Zheng et al. [6, 7] proposed CNT sorting mediated through a poly GT oligonucleotide formed by a non-Watson-Crick hydrogen bond network. A study of adsorption of a GT dimer on

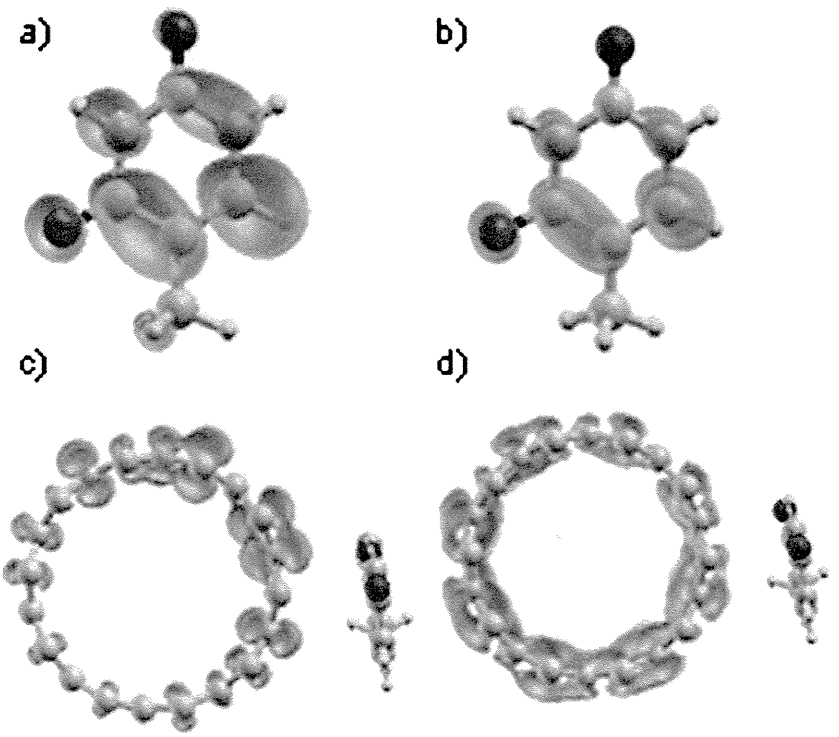

Fig. 4a–d Influence of the intermolecular separation in the charge accumulation and depletion in CNT (10,0) thymine hybrid. **a** HOMO of isolated thymine. **b** LUMO of isolated thymine. **c** HOMO of CNT (10, 0) thymine hybrid. **d** LUMO of CNT (10, 0) thymine hybrid

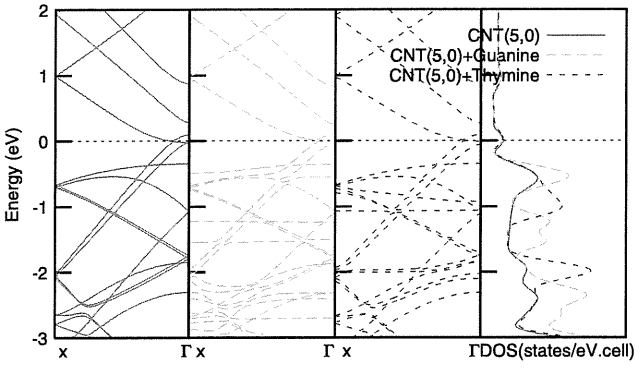

Fig. 5 Comparison between the band structure and density of states of CNT (5, 0), CNT (5, 0) guanine hybrid and CNT (5, 0) thymine hybrid

(11, 0) SWCNT revealed that, due to the stress induced within the ssDNA sugar residues and glycosidic bonds during optimization, the structural geometry was altered and became unstable [8]. In our study, the sugar phosphate backbone of DNA is not taken into account. Initially, the GT base pair is placed parallel to the CNT in the *z*-axis direction. The optimization process rearranged the initial parallel orientation of the base pair. The oxygen- and nitrogen-enriched middle portion of the nucleic acid base pair is moved away from the CNT (Fig. 6). Binding energy of the π–π stacked system is expected to increase in proportional with the π electron surface [30]. The calculated binding energy of the GT base pair with CNT (5, 0) is 0.36 eV. In comparison with the binding energy of isolated guanine (0.41 eV) and thymine (0.20 eV) with CNT (5, 0), the binding strength of the guanine thymine base pair on CNT (5, 0) is relatively weak. Charge density analysis has shown a charge transfer of 0.1e to the CNT from the base pair. The electronic charge density plots of HOMO and LUMO are presented in Fig. 6. In the HOMO (Fig. 6a), charge is distributed over the CNT and oxygen, nitrogen atoms of the nucleic acid bases. Charge of the LUMO (Fig. 6b) is distributed evenly on CNT, which establishes the metallic nature of the tube.

Conclusions

We have studied the interaction mechanism of the nucleic acid bases guanine and thymine with four different CNTs. Apart from the curvature effect of CNT, orientation of the nucleic acid bases and intermolecular distance between CNT and nucleic acid base play a predominant role in deciding the binding strength, which in turn influences charge transfer. Most importantly, the π–π stacking interaction is affected by the intermolecular distance between the CNT and the nucleic acid base. The binding strength of the nucleic acid base is reduced due to the exchange-repulsive interaction of the π–π charge cloud when the intermolecular distance between the adsorbent and adsorbate is less than the characteristic π–π stacking separation. However, the resultant π–π stacking interaction is attractive. When comparing the results obtained for guanine and thymine, the interaction energy of guanine is higher than that of thymine for all the CNTs tested. The role of van der Waals interactions in determining the magnitude of the π–π interaction energy is directly proportional to the area of the π overlap [30]. In addition to the pyrimidine ring of thymine, guanine has a fused imidazole ring and more electronegative nitrogen atoms, increasing the area of π surface of the adsorbate, which enhances the interaction. The binding energy of the adsorbate increases as the diameter of the CNT increases. However, this is not true in the case of guanine adsorption on CNT (5, 0) and thymine adsorption on CNT (10, 0). The high curvature of the narrow CNT (5, 0) drags more electrons towards it, and the contraction of the CNT facilitates the interaction of π electron clouds. This explains the higher binding energy of guanine with the narrow tube rather than the wide tubes. In

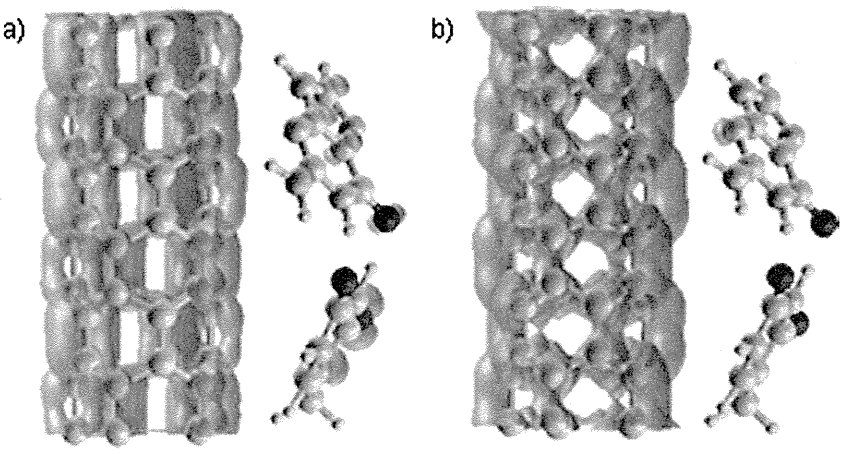

Fig. 6a,b Intermolecular interaction of CNT (5, 0) guanine thymine hybrid. **a** HOMO of CNT (5, 0) guanine thymine hybrid. **b** LUMO of CNT (5, 0) guanine thymine hybrid

the case of CNT (10, 0), the short intermolecular separation between thymine and CNT (10, 0) leads to the reduced binding energy of thymine because of the increased π–π repulsive interaction. Our results confirm that DFT-LDA can forecast the intermolecular separations and binding energies of non-covalent systems. Modeling a bio-nano hybrid like a non-covalently adsorbed nucleic acid base on CNT can lead to the utilization of CNT as a sensor or as a transporter for drugs and genes.

Acknowledgments The University Grants Commission is acknowledged for supporting this project with a junior research fellowship, under University with Potential for Excellence. K.I. acknowledges the financial support of the Council of Scientific and Industrial Research under the Emeritus Scientist Scheme. The authors would like to express their sincere thanks to the crew of the Center for Computational Materials Science at the Institute for Materials Research, Tohoku University, for their continuous support of the SR11000 supercomputing facilities.

References

1. Lu Q, Moore JM, Huang G, Mount AS, Rao AM (2004) RNA polymer translocation with single-walled carbon nanotubes. Nano Lett 4:2473–2477
2. Kam NWS, Dai H (2005) Carbon nanotubes as intracellular protein transporters: generality and biological functionality. J Am Chem Soc 127:6021–6026
3. Chen RJ, Bangsarunzip S, Drouvalakis KA, Shi Kam NW, Shim M, Li Y, Kim W, Utz PJ, Dai H (2003) Noncovalent functionalization of carbon nanotubes for highly specific electronic biosensors. Proc Natl Acac Sci USA 100:4984–4989
4. Kuang Z, Kim SN, Crookes-Goodson WJ, Farmer BL, Naik RR (2010) Biomimetic chemosensor: designing peptide recognition elements for surface functionalization of carbon nanotube field effect transistors. ACS Nano 4:452–458
5. Zheng M, Jagota A, Semke ED, Diner BA, Mclean RS, Lustig SR, Richardson RE, Tassi NG (2003) DNA-assisted dispersion and separation of carbon nanotubes. Nat Mater 2:338–342
6. Zheng M, Jagota A, Strano MS, Santos AP, Barone P, Chou SG, Diner BA, Dresselhaus MS, Mclean RS, Onoa GB, Samsonidze GG, Semke ED, Usrey M, Walls DJ (2003) Structure based carbon nanotube sorting by sequence-dependent DNA assembly. Science 302:1545–1548
7. Tu X, Zheng M (2008) A DNA based approach to the carbon nanotube sorting problem. Nano Res 1:185–194
8. Johnson RR, Charlie Johnson AT, Klein ML (2008) Probing the structure of DNA-carbon nanotube hybrids with molecular dynamics. Nano Lett 8:69–75
9. Lu G, Maragakis P, Kaxiras E (2005) Carbon nanotube interaction with DNA. Nano Lett 5:897–900
10. Meng S, Maragakis P, Papaloukas C, Kaxiras E (2007) DNA nucleoside interaction and identification with carbon nanotubes. Nano Lett 7:45–50
11. Gowtham S, Scheicher RH, Pandey R, Karna SP, Ahuja R (2008) First-principles study of physisorption of nucleic acid bases on small diameter carbon nanotubes. Nanotechnology 19 (6):125701
12. Shukla MK, Dubey M, Zakar E, Namburu R, Czyznikowska Z, Leszczynski J (2009) Interaction of nucleic acid bases with single-walled carbon nanotube. Chem Phys Lett 480:269–272
13. Stepanian SG, Karachevtsev MV, Glamazda AY, Karachevtsev VA, Adamowicz L (2009) Raman spectroscopy study and first-principles calculations of the interaction between nucleic acid bases and carbon nanotubes. J Phys Chem A 113:3621–3629
14. Das A, Sood AK, Maiti PK, Das M, Varadarajan R, Rao CNT (2008) Binding of nucleobases with single-walled carbon nanotubes: theory and experiment. Chem Phys Lett 453:266–273
15. Frischknecht AL, Martin MG (2008) Simulation of the adsorption of nucleotide monophosphates on carbon nanotubes in aqueous solution. J Phys Chem C 112:6271–6278
16. Martin W, Zhu W, Krilov G (2008) Simulation study of noncovalent hybridization of carbon nanotubes by single-stranded DNA in water. J Phys Chem B 112:16076–16089
17. Shtogun YV, Woods LM, Dovbeshko GI (2007) Adsorption of adenine and thymine and their radicals on single-wall carbon nanotubes. J Phys Chem C 111:18174–18181
18. Wang Y (2008) Theoretical evidence for the stringer ability of thymine to disperse SWCNT than cytosine adenine: self stacking bases vs their cross stacking with SWCNT. J Phys Chem C 112:14297–14305
19. Kresse G, Furthmuller J (1996) Efficient iterative schemes for ab initio total-energy calculations using a plane-wave basis set. Phys Rev B 54:11169–11186
20. Kresse G, Furthmuller J (1996) Efficiency of ab initio total energy calculations for metals and semiconductors using a plane-wave basis set. Comput Mater Sci 6:15–50
21. Blochl PE, Kresse G, Joubert J (1999) Projected augmented-wave method. From ultrasoft pseudopotentials to the projector augmented-wave method. Phys Rev B 50:17953–17979
22. Perdew JP, Zunger A (1981) Self-interaction correction to density-functional approximations for many-electron systems. Phys Rev B 23:5048–5079
23. Perdew JP, Chevary JA, Vosko SH, Jackson KA, Pederson MR, Singh DJ, Fiolhais C (1992) Atoms, molecules, solids, and surfaces: applications of the generalized gradient approximation for exchange and correlation. Phys Rev B 46:6671–6687
24. Girifalco LA, Hodak M (2002) Van der Waals binding energies in graphitic structures. Phys Rev B 65(1):125404
25. Tournus F, Latil S, Heggie MI, Charlier JC (2005) π-stacking interaction between carbon nanotubes and organic molecules. Phys Rev B 72(5):075431
26. Ortmann F, Schmidt WG, Bechstedt F (2005) Attracted by long range electron correlation: adenine and graphite. Phys Rev Lett 95 (4):186101
27. Lim S, Park N (2009) Ab initio study of noncovalent sidewall functionalization of carbon nanotubes. Appl Phys Lett 95(3):243110
28. Monkhorst HJ, Pack JD (1976) Special points for brillouin-zone integrations. Phys Rev B 13:5188–5192
29. Liu Z, Sun X, Nakayama-Ratchford N, Dai H (2007) Supramolecular chemistry on water-soluble carbon nanotubes for drug loading and delivery. ACS Nano 1:50–56
30. Hunter CA, Sanders JKM (1990) The nature of π–π interactions. J Am Chem Soc 112:5525–5534
31. Jeziorski B, Moszynski R, Szalewicz K (1994) Perturbation theory approach to intermolecular potential energy surfaces of van der Waals complexes. Chem Rev 94:1887–1930
32. Henkelman G, Arnaldsson A, Jonsson H (2006) A fast and robust algorithm for Bader decomposition of charge density. Comput Mater Sci 36:254–360
33. Kokalj A (2003) Computer graphics and graphical user interfaces as tools in simulations of matter at the atomic scale. Comput Mater Sci 28:155–168

NeuroImage 60 (2012) 471–475

Contents lists available at SciVerse ScienceDirect

NeuroImage

journal homepage: www.elsevier.com/locate/ynimg

Sleep duration during weekdays affects hippocampal gray matter volume in healthy children

Yasuyuki Taki [a,*], Hiroshi Hashizume [a], Benjamin Thyreau [a], Yuko Sassa [a], Hikaru Takeuchi [b], Kai Wu [c], Yuka Kotozaki [b], Rui Nouchi [b], Michiko Asano [a], Kohei Asano [a], Hiroshi Fukuda [c], Ryuta Kawashima [a,b,d]

[a] Division of Developmental Cognitive Neuroscience, Institute of Development, Aging and Cancer, Tohoku University, Sendai 980-8575, Japan
[b] Smart Ageing International Research Centre, Institute of Development, Aging and Cancer, Tohoku University, Sendai 980-8575, Japan
[c] Department of Nuclear Medicine & Radiology, Institute of Development, Aging and Cancer, Tohoku University, Sendai 980-8575, Japan
[d] Department of Functional Brain Imaging, Institute of Development, Aging and Cancer, Tohoku University, Sendai 980-8575, Japan

ARTICLE INFO

Article history:
Received 21 July 2011
Revised 17 November 2011
Accepted 24 November 2011
Available online 14 December 2011

Keywords:
Gray matter
Sleep
Children
Hippocampus
Voxel-based morphometry

ABSTRACT

Sleep is essential for living beings, and sleep loss has been shown to affect hippocampal structure and function in rats by inhibiting cell proliferation and neurogenesis in this region of the brain. We aimed to analyze the correlation between sleep duration and the hippocampal volume using brain magnetic resonance images of 290 healthy children aged 5–18 years. We examined the volume of gray matter, white matter, and the cerebrospinal fluid (CSF) space in the brain using a fully automated and established neuroimaging technique, voxel-based morphometry, which enabled global analysis of brain structure without bias towards any specific brain region while permitting the identification of potential differences or abnormalities in brain structures. We found that the regional gray matter volume of the bilateral hippocampal body was significantly positively correlated with sleep duration during weekdays after adjusting for age, sex, and intracranial volume. Our results indicated that sleep duration affects the hippocampal regional gray matter volume of healthy children. These findings advance our understanding of the importance of sleep habits in the daily lives of healthy children.

Introduction

Although the function of sleep remains debatable, sleep has been associated with the function and structure of the hippocampus. For example, one major theory about the function of sleep proposes that memory consolidation occurs predominantly during sleep, when the hippocampus sends information from memory to the neocortex for permanent storage (Axmacher et al., 2009). Additionally, sleep deprivation was shown to reduce the proliferation of cells and to suppress neurogenesis in the hippocampus of rats (Guzman-Marin et al., 2003, 2005). Even human patients with primary insomnia showed significant reductions in hippocampal volume (Riemann et al., 2007). Although the correlation between sleep and the hippocampus has been elucidated in studies on animals and on human patients and although the influence of chronic sleep loss on the cognition of healthy children has been examined (Jan et al., 2010), the correlation between sleep and the hippocampal volume of healthy children has not yet been clarified. Understanding the correlation between sleep and the hippocampus of children is especially important to identify the sleeping habits associated with the development of a healthy brain and sound cognition. Therefore, we aimed to analyze the correlation between sleep duration and the hippocampal gray matter volume using brain magnetic resonance images of 290 healthy children aged 5–18 years by applying voxel-based morphometry (VBM). This approach enabled global analysis of brain structure and without bias towards any specific brain region while permitting the identification of potential differences or abnormalities in brain structures (Ashburner and Friston, 2000). We hypothesized that there would be a significant positive correlation between sleep duration and the hippocampal gray matter volume in healthy children.

Materials and methods

Participants

All subjects were healthy Japanese children and the detail of the recruitment is written elsewhere (Taki et al., 2010). Briefly, we collected brain MR images from 290 subjects (145 boys, 145 girls; age range, 5.6–18.4 years) who did not have any history of malignant tumors, head traumas with a loss of consciousness lasting over 5 min, developmental disorders, epilepsy, psychiatric diseases, or claustrophobia. We announced that only right-handed children can participate in this study in an advertisement used in the subject recruitment, and also confirmed that all subjects were right-handedness using the self-writing questionnaire "Edinburgh Handedness Inventory" (Oldfield, 1971). We measured full-scale intelligence quotients (IQ) by having trained

* Corresponding author at: Division of Developmental Cognitive Neuroscience, Institute of Development, Aging & Cancer, Tohoku University, 4-1 Seiryocho, Aobaku, 980-8575 Sendai, Japan. Fax: +81 22 717 8457.
E-mail address: ytaki@idac.tohoku.ac.jp (Y. Taki).

1053-8119/$ – see front matter © 2011 Elsevier Inc. All rights reserved.
doi:10.1016/j.neuroimage.2011.11.072

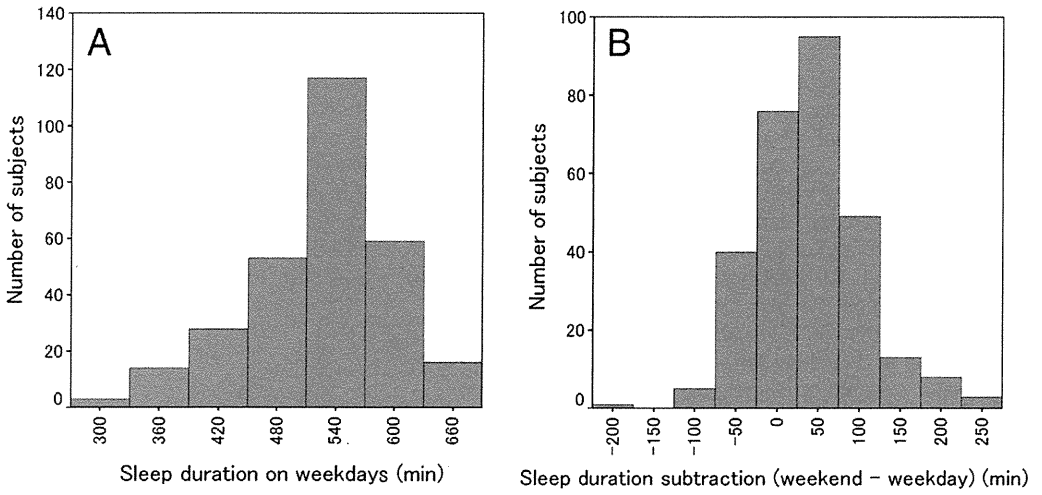

Fig. 1. Histograms showing duration of sleep on weekdays (A) and duration of sleep on weekends minus that on weekdays (B) for all subjects.

examiners administer the Japanese version of the Wechsler Adult Intelligence Scale-Third Edition (WAIS-III) (Fujita, et al., 2006) to subjects aged 16 years or older or the Wechsler Intelligence Scale for Children-Third Edition (WISC-III) to subjects younger than 16 years of age (Azuma, et al., 1998). The duration of sleep during weekdays and that during weekends was collected using self-answering questionnaire, and the duration of sleep during weekdays and the duration of sleep during weekdays subtracted from that during weekends for all subjects are shown in Fig. 1. We did not collect subjective sleep scales, such as sleepiness, from questionnaires or visual analog scales. Instead, we regarded duration of sleep during weekdays subtracted from that during weekends as the subjective scale of sleep. The characteristics of the subjects are shown in Table 1. As per the Declaration of Helsinki (1991), written informed consent was obtained from each subject and his/her parent prior to MR image scanning after a full explanation of the purpose and procedures of the study was provided. Approval for these experiments was obtained from the Institutional Review Board of Tohoku University.

Image acquisition

All images were collected using a 3-T Philips Intera Achieva scanner. Three-dimensional, high-resolution, T1-weighted structural images were collected using a magnetization-prepared rapid gradient-echo (MPRAGE) sequence. The parameters were as follows: 240×240 matrix, TR = 6.5 ms, TE = 3 ms, TI = 711 ms, FOV = 24 cm, 162 slices, 1.0-mm slice thickness, and scan duration of 8 min and 3 s.

Image analysis

Voxel-based morphometry (VBM) with Diffeomorphic Anatomical Registration using Exponentiated Lie Algebra (DARTEL) (Ashburner, 2007) was conducted. DARTEL has been shown to produce a more accurate registration than the standard VBM procedure (Klein et al., 2009) and enables increased sensitivity to findings such as the correlation between gray matter volume and several measures such as age. After image acquisition by MRI, all T1-weighted MR images were analyzed using Statistical Parametric Mapping 8 (SPM8) (Wellcome Department of Cognitive Neurology, London, UK) in Matlab (Math Works, Natick, MA, USA). First, the "New Segmentation" algorithm from SPM8 was applied to every T1-weighted MR image to extract tissue maps corresponding to gray matter, white matter, and cerebrospinal fluid (CSF). This algorithm, which is an improvement on the unified segmentation algorithm (Ashburner and Friston, 2005), uses a Bayesian framework to iteratively perform the probabilistic tissue classification and spatial non-linear deformation in terms of Montreal Neurological Institute (MNI) space. Although we were interested only in the probabilistic tissue segmentation at this point, this new Bayesian segmentation and warping algorithm, which included an improved set of tissue priors (Ashburner and Friston, 2009) for regularization, increased the robustness and accuracy of the segmentation over that of previous standard VBM algorithms. This step allowed us to obtain probability maps of the three aforementioned tissues for each subject and to have them all rigidly registered by ignoring the non-rigid part of the warping to a temporary common space (which happened to be as close to the MNI space as can be reached by a rigid transformation) because the subsequent DARTEL step focused on estimating the "pure non-linear" component of the transformation and used rigidly registered tissues as input. Next, these 290 segmented tissue maps were used to create a customized, more population-specific template using the DARTEL template-creation tool (Ashburner, 2007). DARTEL estimates the best set of smooth deformations working from every subject's tissues to their common average, applies the deformations to create a new average, and then reiterates the process until convergence is achieved. The

Table 1
Characteristics of subjects.

	Boys ($n=144$)	Girls ($n=146$)	P
Age [years], (mean ± SD, range)	11.0 ± 2.87, 5.6–17.1	11.6 ± 3.35, 5.8–18.4	0.100[a]
Full-scale IQ, (mean ± SD, range)	104.3 ± 13.24, 77–137	100.9 ± 11.13, 71–128	0.019[b]
Socioeconomic status[d], (mean, range)	4.04, 1–7	3.85, 1–7	0.252[c]
Sleep duration [min] (mean ± SD, range)	519.0 ± 69.4, 300–660	510.0 ± 75.1, 300–660	0.289[a]
Sleep subtraction[e] [min] (mean ± SD, range)	23.6 ± 61.8, −90–240	52.3 ± 63.6, −205270	<0.001[a]

[a] Student's *t*-test.
[b] Welch's *t*-test.
[c] Mann–Whitney *U*-test.
[d] Socioeconomic status was classified as follows; annual income below 2 million yen, 1; 2–4 million yen, 2; 4–6 million yen, 3; between 6 and 8 million yen, 4, 8–10 million yen, 5; 10–12 million yen, 6; more that 12 million yen, 7.
[e] Sleep subtraction was calculated by subtracting the duration of sleep during weekdays from that during weekends.

smoothness and reversibility of the deformation are obtained from the diffeomorphic properties of DARTEL transformations. The template space was matched to the MNI space using an affine-only registration, which enabled us to match our images' custom coordinate space to the more standard MNI space (Bergouignan et al., 2009). We used a set of standard MNI tissues maps and a multivariate tissue-affinity-registration algorithm provided by SPM and DARTEL for that process. At the end of the process, each subject's gray matter map was warped using its corresponding smooth, reversible deformation parameters to transform it to the custom template space and then to the MNI standard space. We also computed the group means and variances of all these images to visually confirm that the process had operated correctly by searching for a low variance near major landmarks. The major advantage of creating a population-specific template on which to register the tissues is that this approach limits the amount of stretching of each image during the necessary step of spatial normalization. As described by Good et al. (2001), the warped gray matter images were then modulated by calculating the Jacobian determinants derived from the special normalization step and multiplying each voxel by the relative change in volume to obtain the gray matter volume. This modulation step was performed to correct for volume changes in nonlinear normalization. Finally, the warped modulated gray matter images were smoothed by convolving an 8-mm full-width at half-maximum isotropic Gaussian kernel. After completing these image analyses, we obtained smoothed modulated gray matter images to be used for the statistical analysis.

Statistical analysis

We used SPM8 for all statistical analyses. We performed multiple regression analysis, in which regional gray matter volume was used as a dependent variable, and age, sex, duration of sleep, and intracranial volume were used as independent variables to investigate the correlation between hippocampal regional gray matter volume and duration of sleep. Intracranial volume was calculated by summing the gray matter, white matter, and CSF volumes derived from the aforementioned imaging process. We performed region-of-interest (ROI) analysis by setting the ROI of the bilateral hippocampus using the "WFU_PickAtlas" (Lancaster et al., 2000; Maldjian et al., 2003) and performed small-volume correction within the ROI. We set the significance level at $p<0.05$ for the family-wise error rate.

Results

We found that the volume of the bilateral hippocampal body was significantly positively correlated with the duration of sleep during weekdays after adjusting for age, sex, and intracranial volume and after performing small-volume correction of the hippocampal ROI (left: $t=3.59$, $p=0.014$, family-wise error, corrected; right: $t=3.81$, $p=0.007$, family-wise error, corrected), as shown in Fig. 2. The whole-brain analysis showed that the duration of sleep during weekdays was substantially positively correlated with the regional gray matter volume of the bilateral hippocampal body (left: $t=3.59$, $p<0.001$, uncorrected; right: $t=3.81$, $p<0.001$, uncorrected) and the right dorsolateral prefrontal cortex ($t=3.95$, $p<0.001$, uncorrected) after adjusting for age, sex, and intracranial volume and using the liberal threshold ($p<0.001$, uncorrected; cluster size >100). Next, we subtracted the duration of sleep during weekdays from that during weekends. Although we found a significant negative correlation between the duration of sleep during weekdays and the difference between the duration of weekend and weekday sleep (partial correlation coefficient $[C]=-0.300$, $p<0.001$, adjusting for age

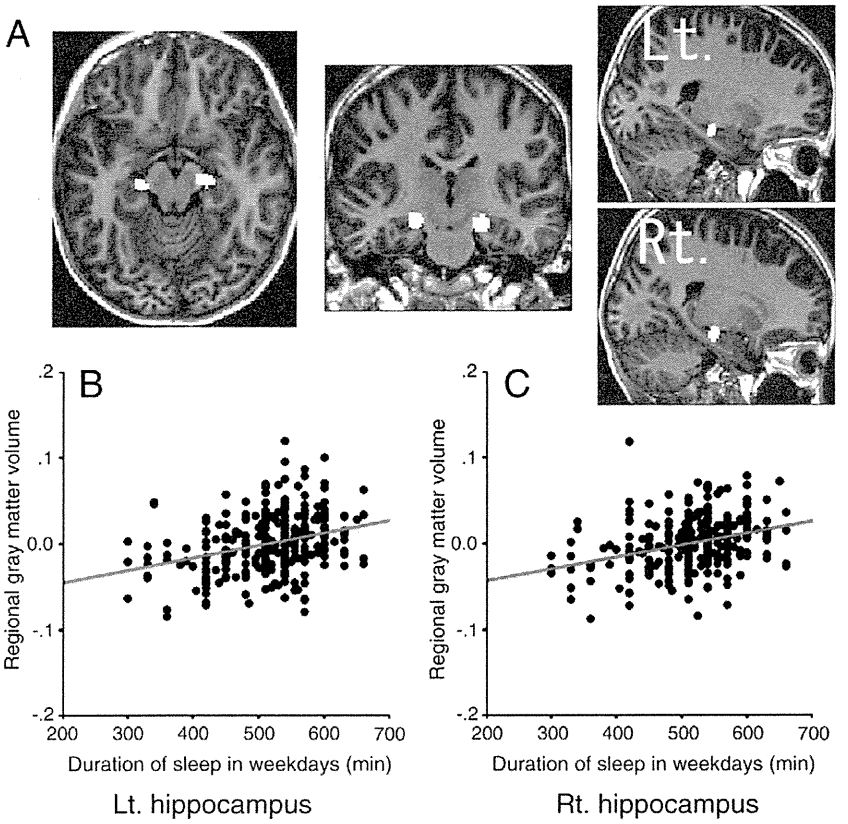

Fig. 2. Correlations between duration of sleep on weekdays and regional gray matter volume in the region-of-interest analysis of the bilateral hippocampus. (A) Gray matter regions showing significant positive correlations between duration of sleep on weekdays and regional gray matter volume according to axial, coronal, and sagittal views. (B) Correlations between duration of sleep on weekdays and regional gray matter volume in the left hippocampus. (C) Correlations between duration of sleep on weekdays and regional gray matter volume in the right hippocampus.

and sex), no significant correlation between regional gray matter volume and this difference remained after adjusting for age, sex, and intracranial volume.

Discussion

We demonstrated that the regional gray matter volume of the bilateral hippocampus was significantly positively correlated with the duration of sleep during weekdays. Although the mechanisms underlying this significant positive correlation have not been clarified, the findings of several studies in rats and humans have supported these results. The generation of new neurons in dentate gyrus of the hippocampus has been confirmed in several mammals, including humans (Eriksson et al., 1998; Gould et al., 1999). However, sleep deprivation reduced the proliferation of cells in the dentate gyrus of the hippocampus (Guzman-Marin et al., 2003) and also suppressed neurogenesis in rats (Guzman-Marin et al., 2005). Even human patients with primary insomnia showed significantly smaller bilateral hippocampal volumes than did good sleepers after adjusting for age and sex (Riemann et al., 2007). Moreover, patients with obstructive sleep apnoea, a common sleep disorder, showed significant gray matter reduction in several regions such as the hippocampus (Canessa et al., 2011; Macey et al., 2002). In addition to these findings, the role of sleep may modulate synaptic contacts by downscaling synaptic strength to a baseline level that is energetically sustainable, which is beneficial for maintaining plasticity for a new environment and, as a result, learning and memory (Tononi and Cirelli, 2006). Specifically, sleep deprivation affects hippocampal activation and decreases memory performance (Van Der Werf et al., 2009; Yoo et al., 2007). Thus, sleep may be necessary, at the very least, for neurogenesis and for synaptic reorganization in the human hippocampus.

We did not find a significant correlation between regional gray matter volume and the difference between the duration of sleep during weekdays and that during weekends. A recent study proposed that the quality and the duration of sleep should be regarded as two separate domains – the subjective and objective, respectively – even though these domains do overlap to some extent (Dewald et al., 2010). As mentioned above, because the duration of sleep constitutes an objective aspect of sleep, we also analyzed the correlation between regional gray matter volume and the subjective (qualitative) aspect of sleep using the difference between weekday and weekend sleep duration. Our rationale was as follows. Given that school starts at about 8:30 AM on weekdays in Japan, weekday times of awakening are determined by school schedules; however, most Japanese children do not attend school during weekends. Thus, if the quality of sleep were low during the week, we would expect children to awaken later during weekends. For this reason, the subtraction process described above was employed to reflect the quality of sleep (a subjective aspect) during weekdays. The absence of a significant correlation between regional gray matter volume and the result of this calculation indicated that hippocampal volume is more crucial for the objective than for the subjective aspect of sleep. Thus, more sleep may be more beneficial for the hippocampus irrespective of the subjective aspects of sleep. However, we cannot conclude that excessive sleep would have a positive effect on hippocampal and cognitive functioning given that the number of the subjects demonstrating excessive amounts of sleep was rather small, as shown in Fig. 1. Indeed, the mean sleep duration of subjects in this study was 8.57 h, which approximates empirical evidence showing that children and adolescents require, on average, approximately 9 h of sleep per night (Mercer et al., 1998). Additionally, the mean difference between the duration of sleep during weekends and that during weekdays was 38 min in favor of weekends, which we evaluated as rather small. Thus, we believe that the duration of sleep obtained by the subjects in this study was generally appropriate, and we concluded that sufficient, but not excessive, sleep is beneficial for the hippocampus.

We found that the regional gray matter volume of the right dorsolateral prefrontal cortex had a substantial positive correlation with the duration of sleep during weekdays in the whole-brain analysis. Although we did not find the mechanism of the correlation, it is thought that maturational pattern of the dorsolateral prefrontal cortex is a plausible mechanism to account for the correlation. Postmortem studies of human brains showed that the time course of synaptogenesis was earlier in the visual cortex and auditory cortex than in the prefrontal cortex (Huttenlocher, 1979; Huttenlocher and Dabholkar, 1997; Huttenlocher et al., 1982). In addition, synapse elimination starts earlier in the visual cortex than in the auditory cortex, and that in the prefrontal cortex starts later than in both of the former regions (Huttenlocher and Dabholkar, 1997). These results suggest that brain maturation starts in the occipital lobe, and then moves to the temporal lobe, followed by the prefrontal cortex. In addition, recent neuroimaging studies have shown that brain gray matter maturation progresses with an increase in volume followed by a decrease in volume (Courchesne et al., 2000; Giedd et al., 1999; Gogtay et al., 2004; Shaw et al., 2008), which is thought to be related to synaptogenesis and synaptic elimination (Huttenlocher and Dabholkar, 1997) and with intracortical myelination (Paus, 2005), and the prefrontal cortex is known as one of the latest maturing regions (Gogtay et al., 2004). Because the period corresponding to the highest gray matter volume and brain perfusion of the prefrontal cortex is around adolescence (Gogtay et al., 2004; Taki et al., 2011), the dorsolateral prefrontal cortex may be especially affected by sleep pattern from the childhood to adolescence. Because the dorsolateral prefrontal gyrus is involved in higher cognitive functions, such as working memory (Baddeley, 2003; Klingberg, 2006) and executive function (Kramer et al., 2007; Zimmerman et al., 2006), sufficient sleep is thought to be important for several cognitive functions.

The present study had limitations. First, this is a cross-sectional study. Thus, although we have shown a relationship between sleep duration and hippocampal gray matter volume, we cannot clarify a causal relationship between sleep and hippocampal gray matter volume. Longitudinal studies are needed to clarify this issue. Second, as for the subjective sleepiness, we evaluated the subjective (qualitative) aspect of sleep using the difference between weekday and weekend sleep duration; however, we did not collect data on subjective sleepiness directly, such as asking whether the subjects felt sleepy during the daytime using questionnaires or visual analog scale. Therefore, further studies may help to clarify the correlation between subjective aspects of sleep, such as sleepiness, and brain structure.

In conclusion, our brain MRI study demonstrated that the duration of sleep during weekdays was significantly positively correlated with the regional gray matter volume of the bilateral hippocampus, suggesting that sufficient sleep has a beneficial effect on the hippocampus. These findings advance our understanding of the importance of sleep habits in the daily lives of children.

Acknowledgments

We thank Y. Yamada for collecting MR data, and Y. Suzuki for technical support. This work was supported by a Ministry of Education, Culture, Sports, Science and Technology Grant-in-Aid for Young Scientists (B) (grant number 20790875).

References

Ashburner, J., 2007. A fast diffeomorphic image registration algorithm. NeuroImage 38, 95–113.
Ashburner, J., Friston, K.J., 2000. Voxel-based morphometry—the methods. NeuroImage 11, 805–821.
Ashburner, J., Friston, K.J., 2005. Unified segmentation. NeuroImage 26, 839–851.
Ashburner, J., Friston, K.J., 2009. Computing average shaped tissue probability templates. NeuroImage 45, 333–341.

Axmacher, N., Draguhn, A., Elger, C.E., Fell, J., 2009. Memory processes during sleep: beyond the standard consolidation theory. Cell. Mol. Life Sci. 66, 2285–2297.
Azuma, H., Ueno, K., Fujita, K., Maekawa, H., Ishikuma, T., Sano, H., 1998. Japanese Wechsler Intelligence Scale for Children, 3rd ed. Nihon Bunka Kagakusha, Tokyo.
Baddeley, A., 2003. Working memory: looking back and looking forward. Nat. Rev. Neurosci. 4, 829–839.
Bergouignan, L., Chupin, M., Czechowska, Y., Kinkingnehun, S., Lemogne, C., Le Bastard, G., Lepage, M., Garnero, L., Colliot, O., Fossati, P., 2009. Can voxel based morphometry, manual segmentation and automated segmentation equally detect hippocampal volume differences in acute depression? NeuroImage 45, 29–37.
Canessa, N., Castronovo, V., Cappa, S.F., Aloia, M.S., Marelli, S., Falini, A., Alemanno, F., Ferini-Strambi, L., 2011. Obstructive sleep apnea: brain structural changes and neurocognitive function before and after treatment. Am. J. Respir. Crit. Care Med. 183, 1419–1426.
Courchesne, E., Chisum, H.J., Townsend, J., Cowles, A., Covington, J., Egaas, B., Harwood, M., Hinds, S., Press, G.A., 2000. Normal brain development and aging: quantitative analysis at in vivo MR imaging in healthy volunteers. Radiology 216, 672–682.
Dewald, J.F., Meijer, A.M., Oort, F.J., Kerkhof, G.A., Bogels, S.M., 2010. The influence of sleep quality, sleep duration and sleepiness on school performance in children and adolescents: a meta-analytic review. Sleep Med. Rev. 14, 179–189.
Eriksson, P.S., Perfilieva, E., Bjork-Eriksson, T., Alborn, A.M., Nordborg, C., Peterson, D.A., Gage, F.H., 1998. Neurogenesis in the adult human hippocampus. Nat. Med. 4, 1313–1317.
Fujita, K., Maekawa, H., Dairoku, H., Yamanaka, K., 2006. Japanese Wechsler Adult Intelligence Scale, 3rd ed. Nihon Bunka Kagakusha, Tokyo.
Giedd, J.N., Blumenthal, J., Jeffries, N.O., Castellanos, F.X., Liu, H., Zijdenbos, A., Paus, T., Evans, A.C., Rapoport, J.L., 1999. Brain development during childhood and adolescence: a longitudinal MRI study. Nat. Neurosci. 2, 861–863.
Gogtay, N., Giedd, J.N., Lusk, L., Hayashi, K.M., Greenstein, D., Vaituzis, A.C., Nugent III, T.F., Herman, D.H., Clasen, L.S., Toga, A.W., Rapoport, J.L., Thompson, P.M., 2004. Dynamic mapping of human cortical development during childhood through early adulthood. Proc. Natl. Acad. Sci. U. S. A. 101, 8174–8179.
Good, C.D., Johnsrude, I.S., Ashburner, J., Henson, R.N.A., Friston, K.J., Frackowiak, R.S.J., 2001. A voxel-based morphometric study of ageing in 465 normal adult human brains. NeuroImage 14, 21–36.
Gould, E., Reeves, A.J., Fallah, M., Tanapat, P., Gross, C.G., Fuchs, E., 1999. Hippocampal neurogenesis in adult Old World primates. Proc. Natl. Acad. Sci. U. S. A. 96, 5263–5267.
Guzman-Marin, R., Suntsova, N., Stewart, D.R., Gong, H., Szymusiak, R., McGinty, D., 2003. Sleep deprivation reduces proliferation of cells in the dentate gyrus of the hippocampus in rats. J. Physiol. (Lond) 549, 563–571.
Guzman-Marin, R., Suntsova, N., Methippara, M., Greiffenstein, R., Szymusiak, R., McGinty, D., 2005. Sleep deprivation suppresses neurogenesis in the adult hippocampus of rats. Eur. J. Neurosci. 22, 2111–2116.
Huttenlocher, P.R., 1979. Synaptic density in human frontal cortex– developmental changes and effects of aging. Brain Res. 163, 195–205.
Huttenlocher, P.R., Dabholkar, A.S., 1997. Regional differences in synaptogenesis in human cerebral cortex. J. Comp. Neurol. 387, 167–178.
Huttenlocher, P.R., de Courten, C., Garey, L.J., Van der Loos, H., 1982. Synaptogenesis in human visual cortex–evidence for synapse elimination during normal development. Neurosci. Lett. 33, 247–252.
Jan, J.E., Reiter, R.J., Bax, M.C., Ribary, U., Freeman, R.D., Wasdell, M.B., 2010. Long-term sleep disturbances in children: a cause of neuronal loss. Eur. J. Paediatr. Neurol. 14, 380–390.
Klein, A., Andersson, J., Ardekani, B.A., Ashburner, J., Avants, B., Chiang, M.C., Christensen, G.E., Collins, D.L., Gee, J., Hellier, P., Song, J.H., Jenkinson, M., Lepage, C., Rueckert, D., Thompson, P., Vercauteren, T., Woods, R.P., Mann, J.J., Parsey, R.V., 2009. Evaluation of 14 nonlinear deformation algorithms applied to human brain MRI registration. NeuroImage 46, 786–802.
Klingberg, T., 2006. Development of a superior frontal-intraparietal network for visuo-spatial working memory. Neuropsychologia 44, 2171–2177.
Kramer, J.H., Mungas, D., Reed, B.R., Wetzel, M.E., Burnett, M.M., Miller, B.L., Weiner, M.W., Chui, H.C., 2007. Longitudinal MRI and cognitive change in healthy elderly. Neuropsychology 21, 412–418.
Lancaster, J.L., Woldorff, M.G., Parsons, L.M., Liotti, M., Freitas, C.S., Rainey, L., Kochunov, P.V., Nickerson, D., Mikiten, S.A., Fox, P.T., 2000. Automated Talairach atlas labels for functional brain mapping. Hum. Brain Mapp. 10, 120–131.
Macey, P.M., Henderson, L.A., Macey, K.E., Alger, J.R., Frysinger, R.C., Woo, M.A., Harper, R.K., Yan-Go, F.L., Harper, R.M., 2002. Brain morphology associated with obstructive sleep apnea. Am J Respir Crit Care Med 166, 1382–1387.
Maldjian, J.A., Laurienti, P.J., Kraft, R.A., Burdette, J.H., 2003. An automated method for neuroanatomic and cytoarchitectonic atlas-based interrogation of fMRI data sets. NeuroImage 19, 1233–1239.
Mercer, P.W., Merritt, S.L., Cowell, J.M., 1998. Differences in reported sleep need among adolescents. J. Adolesc. Health 23, 259–263.
Oldfield, R.C., 1971. The assessment and analysis of handedness: the Edinburgh inventory. Neuropsychologia 9, 97–113.
Paus, T., 2005. Mapping brain maturation and cognitive development during adolescence. Trends Cogn. Sci. 9, 60–68.
Riemann, D., Voderholzer, U., Spiegelhalder, K., Hornyak, M., Buysse, D.J., Nissen, C., Hennig, J., Perlis, M.L., van Elst, L.T., Feige, B., 2007. Chronic insomnia and MRI-measured hippocampal volumes: a pilot study. Sleep 30, 955–958.
Shaw, P., Kabani, N.J., Lerch, J.P., Eckstrand, K., Lenroot, R., Gogtay, N., Greenstein, D., Clasen, L., Evans, A., Rapoport, J.L., Giedd, J.N., Wise, S.P., 2008. Neurodevelopmental trajectories of the human cerebral cortex. J. Neurosci. 28, 3586–3594.
Taki, Y., Hashizume, H., Sassa, Y., Takeuchi, H., Asano, M., Asano, K., Kawashima, R., 2010. Breakfast staple types affect brain gray matter volume and cognitive function in healthy children. PLoS One 5, e15213 [Electronic Resource].
Taki, Y., Hiroshi, H., Sassa, Y., Takeuchi, H., Wu, K., Asano, M., Asano, K., Fukuda, H., Kawashima, R., 2011. Correlation between gray matter density-adjusted brain perfusion and age using brain MR images of 202 healthy children. Human Brain Mapping 32, 1973–1985.
Tononi, G., Cirelli, C., 2006. Sleep function and synaptic homeostasis. Sleep Medicine Reviews 10, 49–62.
Van Der Werf, Y.D., Altena, E., Schoonheim, M.M., Sanz-Arigita, E.J., Vis, J.C., De Rijke, W., Van Someren, E.J., 2009. Sleep benefits subsequent hippocampal functioning. Nat. Neurosci. 12, 122–123.
Yoo, S.S., Hu, P.T., Gujar, N., Jolesz, F.A., Walker, M.P., 2007. A deficit in the ability to form new human memories without sleep. Nat. Neurosci. 10, 385–392.
Zimmerman, M.E., Brickman, A.M., Paul, R.H., Grieve, S.M., Tate, D.F., Gunstad, J., Cohen, R.A., Aloia, M.S., Williams, L.M., Clark, C.R., Whitford, T.J., Gordon, E., 2006. The relationship between frontal gray matter volume and cognition varies across the healthy adult lifespan. Am. J. Geriatr. Psychiatry 14, 823–833.

Cellular and Molecular Bioengineering, Vol. 4, No. 3, September 2011 *(© 2011)* pp. 327–339
DOI: 10.1007/s12195-011-0183-x

Advances in Experiments and Modeling in Micro- and Nano-Biomechanics: A Mini Review

MIAN LONG,[1] MASAAKI SATO,[2] CHWEE TECK LIM,[3] JIANHUA WU,[4] TAIJI ADACHI,[5] and YASUHIRO INOUE[5]

[1]Key Laboratory of Microgravity, Center of Biomechanics and Bioengineering, Institute of Mechanics, Chinese Academy of Sciences, Beijing 100190, China; [2]Graduate School of Biomedical Engineering, Tohoku University, Sendai 980-8579, Japan; [3]Division of Bioengineering, Department of Mechanical Engineering, Mechanobiology Institute, National University of Singapore, Singapore 117576, Singapore; [4]Institute of Biomechanics, School of Bioscience and Bioengineering, South China University of Technology, Guangzhou, China; and [5]Institute for Frontier Medical Sciences, Kyoto University, Kyoto, Japan

(Received 2 April 2011; accepted 3 June 2011; published online 15 June 2011)

Associate Editor Edward Guo oversaw the review of this article.

Abstract—Recent advances in micro- and nano-technologies and high-end computing have enabled the development of new experimental and modeling approaches to study biomechanics at the micro- and nano-scales that were previously not possible. These new cutting-edge approaches are contributing toward our understanding in emerging areas such as mechanobiology and mechanochemistry. Another important potential contribution lies in translational medicine, since biomechanical studies at the cellular and molecular levels have direct relevance in areas such disease diagnosis, nano-medicine and drug delivery. Thus, the developed experimental and modeling approaches are critical in elucidating important mechanistic insights in both basic sciences and clinical treatment. While it is hard to cover all the recent advances in this mini-review, we focus on several important approaches. For experimental techniques, we review the assays involving shear flow, cellular imaging, microbead, microcontact printing, and micropillars at the micro-scale, and micropipette aspiration, optical tweezers, parallel flow chamber, and atomic force microscopy at the nano-scale. In modeling and simulations, we outline the theoretical modeling for actin dynamics in migrating cell and actin-based cell motility in cellular mechanics, as well as the receptor–ligand binding in cell adhesion and the application of free, steered, and flow molecular dynamics simulations in molecular biomechanics. Relevant scientific issues and applications are also discussed.

Keywords—Cellular mechanics, Molecular biomechanics, Experimental techniques, Theoretical modeling, Computations.

Address correspondence to Mian Long, Key Laboratory of Microgravity, Center of Biomechanics and Bioengineering, Institute of Mechanics, Chinese Academy of Sciences, Beijing 100190, China; Masaaki Sato, Graduate School of Biomedical Engineering, Tohoku University, Sendai 980-8579, Japan; Chwee Teck Lim, Division of Bioengineering, Department of Mechanical Engineering, Mechanobiology Institute, National University of Singapore, Singapore 117576, Singapore. Electronic mails: mlong@imech.ac.cn, sato@bml.mech.tohoku.ac.jp, ctlim@nus.edu.sg

INTRODUCTION

Cells are constantly subjected to and regulated by both chemical and physical factors in its microenvironment. In particular, these physical factors include mechanical forces as well as topography and elasticity of the extracellular matrix. As such, studying biomechanics at the cellular and molecular levels is important to our understanding of how such physical or mechanical factors regulate cell functions in both health and disease. With the recent advances in micro- and nano-technologies as well as high-end computing, we are observing a burgeoning of new experimental and computational approaches to study the biomechanics of biological systems at the micro- and nano-scales. These new and cutting-edge approaches are also fostering a stronger integration between the disciplines of biomechanics and modern biology (cell and molecular biology, genomics, proteomics and systems biology), and allows engineers, physicists, chemists, and biologists to collectively address fundamental issues at the cellular and molecular levels. The knowledge acquired and the cutting-edge technologies developed are also helpful in translating the discoveries in this basic biomechanical study into useful applications in molecular and cell engineering and even in developing novel approaches to diagnose and treat diseases. This mini-review summarizes some of the recent advances in experimental and computational approaches in the field of cellular and molecular mechanics and discusses how they can contribute toward addressing important issues in mechanobiology and mechanochemistry.

Considering the fact that thousands of bioengineers have put tremendous efforts into these areas in the past century, it is very challenging to cover all the

fundamental and important advancements in the mini-review. Here we focus on four aspects: (1) cellular biomechanics techniques including shear flow assay, cellular imaging, and microfabricated technologies for cell mechanics, (2) modeling and simulation of sub-cellular mechanics of cell migration and motility, (3) molecular biomechanics techniques including micro-pipette aspiration, optical tweezers, parallel flow chamber, and atomic force microscopy, and (4) molecular dynamics simulation and mathematical modeling of individual molecule or molecular complex. We hope to showcase the latest contributions not only from around the world, but also from that of the Asian community.

CELL MECHANICS AND MECHANOBIOLOGY

In general, cell mechanics refers to how the elastic and adhesive properties of cells are changed and/or regulated under various physiological and pathological conditions, while mechanobiology refers to how mechanical cues (e.g., shear flow, geometrical patterns, substrate topography and elasticity, etc) elicit various biological responses and functions.

Experimental Techniques

Shear Flow Assay

Fluid flow is one of the important environmental components that a cell may be subjected to. Examples include endothelial and smooth muscle cells in blood and lymph vessels, osteoblasts and osteoclasts cells in bone, and epithelial cells in esophagus and intestines. These cells are continually exposed to flow of blood, lymph, tissue fluid, and digested food among others, in which the physical forces exerted do evoke or regulate cell functions. Fluid flow can be divided into two major types: laminar and turbulent. Various types of devices have been developed to apply fluid flow to cultured cells *in vitro*, depending on their different objectives. There have been many reports focusing on vascular endothelial cells (ECs) exposed to fluid flow or fluid shear stress (FSS). Hemodynamic FSS acting on vascular ECs evokes a variety of cellular responses, including proliferation,[53] expression of adhesive molecules,[70] cytoskeletal structures and morphology,[29] and mechanical properties,[84] that may be relevant to both the physiology and pathology of blood vessels. Many previous studies have attempted to determine the mechanisms by which ECs sense FSS and adapt to such mechanical factors. Here we summarize the devices and image analysis being employed in these studies.

The major devices for subjecting cultured cells to laminar flow are the rotating disk type and parallel-plate flow chamber type.

In the rotating disk devices, there are the parallel-disk[74] and cone-plate[22] types. Shear stress, τ, to be applied to cells in the parallel plate type is expressed as follows, $\tau = \mu r\omega/h$, where μ is the viscosity of fluid, r the distance from the axis of rotation, ω the angular velocity, and h the distance between the two parallel plates. Characteristics of this device are values of shear stress that are dependent upon the distance from the rotational axis. In the case of the cone-plate type, since the distance h between the two surfaces of cone and plate is a function of r and α (angle between the cone and the plate) where $h = r \tan \alpha$, shear stress is constant regardless of position and can be expressed as, $\tau = \mu\omega/\tan \alpha$. The rotating devices are usually used to attain unsteady or turbulent flow by applying high rotating speed and cone angle.[17]

The parallel-plate flow chamber[27,42,52] is commonly used to apply shear stress to cultured cells. Shear stress exerted on the cell surface can be expressed by the equation, $\tau = 6Q\mu/bh^2$, where Q is flow rate and b and h are the width and height of the flow channel, respectively. Various types of flow chamber have been designed to allow for a wide range of shear stress by changing the width[50,95] and height.[65] In addition, the effects of disturbed flow can also be examined in the parallel-plate flow chamber by adding a step in the channel.[16,21,71] Some experiments were focused on examining the impact of spatial gradient of shear stress within the chamber. To obtain the high spatial gradient, *T*-shaped flow chamber was developed and utilized from the viewpoint of genesis and growth of cerebral aneurysm.[82,89]

Cellular Imaging

Recently, FSS-induced activation of several candidates of mechanosensitive molecules, such as G proteins[83] and PECAM,[85] has been demonstrated. However, there is no primary evidence as to whether these molecules are activated directly by mechanical loading or by intracellular signaling interactions that were prompted by another mechanosensor. This comes from the difficulties in precisely describing the intracellular mechanical conditions, i.e., how FSS acting on the apical surface of ECs is transmitted and generates an intracellular mechanical field. As such, it is necessary to investigate the degree to which forces are exerted on the intercellular junction, focal adhesion, and other candidates for mechanotransducers.

In an attempt to solve this problem, Ueki *et al.*[93] developed a novel experimental technique that enables the direct observation of the passive deformation of